2022

Development and Validation of an Accumulator Liquid-Level Estimator to Enable Zero-Superheat and Active Charge Control in Vapor-Compression Systems

Haopeng Liu

Jie Cai

Development and validation of an accumulator liquid-level estimator to enable zero-superheat and active charge control in vapor-compression systems

Haopeng Liu[1], Jie Cai[2]

[1] School of Aerospace and Mechanical Engineering, University of Oklahoma,
Norman, OK, US
Haopeng.Liu-1@ou.edu, jcai@ou.edu

ABSTRACT

Accumulators are commonly used to intercept liquid refrigerant before it reaches the compressor and can also be used as a refrigerant reservoir to assist active charge management. For zero-superheat and active charge control, accurate measurement or estimation of the accumulator liquid level is required. This paper presents an accumulator liquid level estimation approach based on a nonlinear state observer combined with a gray-box dynamic model of the evaporator and accumulator. This approach affords virtual detection of the liquid level in real-time from refrigerant pressure and temperature measurements, which are readily available in modern vapor-compression systems, and supports zero-superheat and dynamic charge control to maximize system efficiency. Both numerical and experimental tests of the proposed liquid level estimation and charge control strategies were carried out with a 3-ton variable-speed heat pump. The tests have demonstrated the accuracy of the accumulator liquid level estimator and shown that the zero-superheat and active charge control strategy could improve the system efficiency by up to 10.5%.

1. INTRODUCTION

Vapor compression system-based loads, such as air conditioning, refrigeration and heat pump space heating, account for more than 20% of total electricity consumption in the U.S (EIA, 2020). Therefore, measures to improve energy efficiency of VCS play a critical role for the transition to a more sustainable and resilient energy economy, and have attracted tremendous research attention in the past few decades.

Superheat is one of the most important control parameters in VCS that affects both system efficiency and reliability. Lower superheat settings can improve the system coefficient of performance (COP), but an excessively low superheat may cause control problems including instability, loss of observability and wet compression that can result in compressor damages (Chen et al., 2002, Jensen and Skogestad, 2007, Kim and Braun, 2012).

The VCS energy efficiency is also highly dependent on the refrigerant charge. Research studies have shown that over- or under-charging the system can reduce the system efficiency by as much as 16% (Choi and Kim, 2002). Relationships between the charge level and system COP were found to exhibit a concave curve with the peak COP occurring at an intermediate charge level (Kim and Braun, 2012). Therefore, bulk of previous studies on refrigerant charge aimed to identify the optimal charge level of a VCS that can inform field technicians or manufacturers in determining how much refrigerant should be added to the system under the rated conditions.

If the active charge can follow the dynamically varying optimal charge, the time-averaged system efficiency can be significantly enhanced. Dynamic active charge management can be achieved by proper control of the inlet conditions of refrigerant tanks, e.g. the high-side receiver or low-side accumulator, which are commonly used in the VCS as a means of storing excess refrigerant and ensuring safe operations. Prior studies made attempts to use both the receiver and accumulator for dynamic active charge control. For example, Jensen and Skogestad (2007) utilized the receiver at the outlet of the condenser to hold excess refrigerant and added an extra valve before the receiver to adjust the refrigerant liquid level therein and to achieve the desired subcooling. The study found that a subcooling of 5K could provide 2% COP improvement compared to a zero subcooling for the specific operating condition under study. Koeln and Alleyne (2014) considered a similar system configuration and proposed two strategies for determination of the optimal active charge that maximizes the system COP. The first strategy identifies the subcooling corresponding to the optimal active charge using an offline simulation analysis and uses a PI controller to modulate the electronic expansion valve (EXV) upstream of the receiver to achieve the desired subcooling. The second strategy adopts the extreme seeking control (ESC) approach as an online model-free optimizer that directly drives the EXV opening to the COP maximizing point. The latter strategy is suitable for practical implementations as it allows online control optimization of systems with

unknown dynamics. However, the dither signal used by the ESC results in constant actuation of the EXV which can significantly impact its lifespan. Both simulation and experimental tests showed that a 9% improvement in the system efficiency could be achieved compared to a conventional operation strategy with zero subcooling. These studies proved the effectiveness of using receivers for active charge management. The dual EXV design allows simultaneous control of the superheat and subcooling which can offer ample performance enhancement. However, only subcooling was controlled in the aforementioned studies.

The dynamics of the low-pressure accumulator and its use for charge management have also been studied. Eldredge et al. (2008) established a dynamic model for the evaporator and accumulator set using the moving-boundary approach, targeting dynamic control and stability analysis. Kim and Braun (2012) added accumulators in air conditioning and heat pump systems as a means to change the system active charge, allowing experimental assessments of the impact of charge level on the system energy efficiency under different combinations of indoor and outdoor temperatures.

A key prerequisite for practical implementations of zero-superheat and active charge control is the ability to reliably estimate the refrigerant liquid level in the accumulator. Adding liquid level detectors in the accumulator is cost prohibitive and can adversely impact system reliability. This paper presents a "virtual" accumulator liquid level detection technique based on a nonlinear state observer combined with a gray-box dynamic model of the evaporator and accumulator set. This technique offers a pure software solution to estimate the liquid level of an accumulator in real-time from sensor readings that are readily available in modern VCSs. The liquid level estimator can be combined with zero-superheat and active charge control to maximize the system efficiency. Both numerical and experimental tests were carried out with a 3-ton variable-speed heat pump and the key test results are reported in this study. To the authors' knowledge, this is the first development of a virtual liquid level detector and also the first study demonstrating its performance in zero-superheat and active charge control.

2. DESCRIPTIONS OF TEST UNIT AND EXPERIMENTAL RIG

The test unit is a split variable-speed direct expansion (DX) system with a rated cooling capacity of 3 tons. The indoor unit contains an A-shaped evaporator coil, an electronically commutated motor-driven supply fan and an EXV upstream of the evaporator, while the outdoor unit packages a variable-speed scroll compressor, a suction accumulator and the condenser coil.

A schematic diagram of the sensors installed on the test unit is shown in Figure 1. The system uses R410A as the refrigerant. Sensors are in place to measure key operation variables such as pressures, temperatures and volumetric flow rates, etc. In Figure 1, letters 'E' and 'C' denote the sensing points for the evaporator and condenser, respectively; 'I' and 'O' indicate the inlet and outlet of a heat exchanger, respectively; 'R' and 'A' represent the refrigerant- and air-side measurements. 'T' and 'P' represent the temperature measurement via thermocouples and pressure transducers, respectively. 'SUC' and 'DIS' represent the suction- and discharge-port measurements. Additional sensors that are not shown in Figure 1 include indoor and outdoor fans, as well as air-side humidity sensors. Details of the experimental setup and the sensors' technical information can be found in Liu and Cai (2021b).

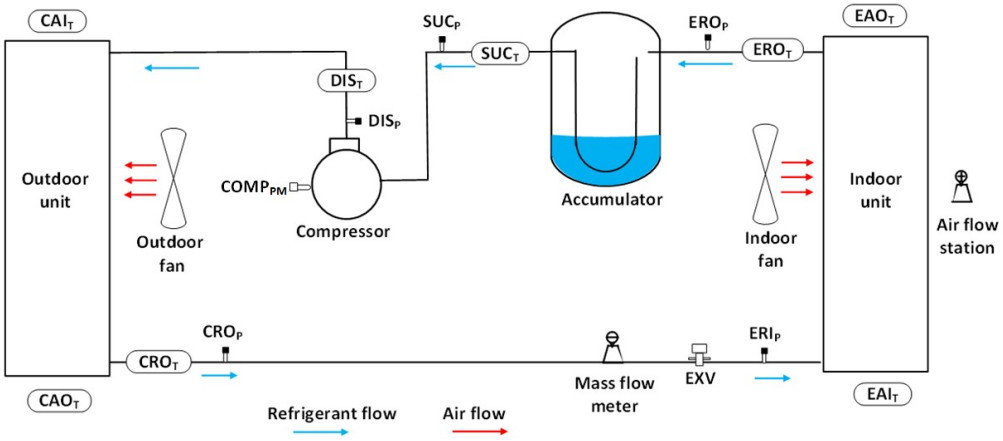

Figure 1: Sensor instrumentation diagram for the test unit.

3. VAPOR COMPRESSION SYSTEM DYNAMIC MODELS

This section introduces two sets of dynamic models: a low-order dynamic model for the evaporator and accumulator set that is used in the liquid level estimator (referred to as control model), and a high-fidelity VCS model in support of simulation-based assessments of the proposed estimation and control strategies. The latter will be referred to as plant model in this paper.

3.1 Low-order model for state estimation

The low-order control model used for state estimation captures the dynamics of the evaporator and accumulator. These component models are elaborated in the following subsections.

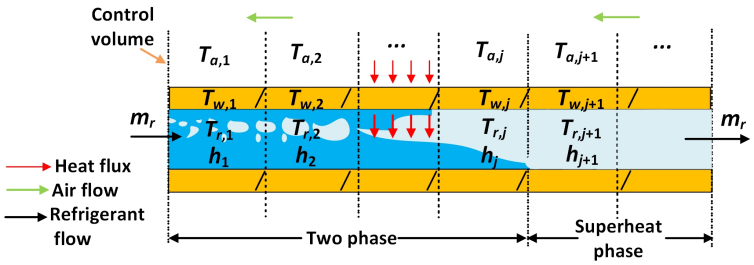

Figure 2: Schematic diagram for a counter-flow, finite control volume model of the evaporator.

3.1.1 Evaporator

A finite control volume approach is adopted for modeling of the evaporator, which divides the heat exchanger into multiple control volumes and applies energy and mass balances to each control volume. A schematic diagram of the modeling method is given in Figure 2. For the j^{th} control volume, the following differential equations characterize the conservation of refrigerant energy, mass and tube wall energy:

$$\dot{U}_j = m_{j-1}h_{j-1} - m_j h_j + \alpha_{r,j}A_{i,j}\left(T_{w,j} - T_{r,j}\right) \tag{1}$$

$$\dot{m}_{e,j} = m_{j-1} - m_j \tag{2}$$

$$\dot{E}_j = \left(C_{th,w}\right)_j \dot{T}_{w,j} = \alpha_{a,j}A_{o,j}\left(T_{a,j} - T_{w,j}\right) - \alpha_{r,j}A_{i,j}\left(T_{w,j} - T_{r,j}\right) \tag{3}$$

where U_j is the refrigerant internal energy; $\alpha_{r,j}$ and $\alpha_{a,j}$ represent the refrigerant- and air-side heat transfer coefficients (HTC), respectively; $A_{i,j}$ and $A_{o,j}$ are the inner and outer heat transfer areas of the j^{th} section of the exchanger, respectively; $T_{w,j}$, $T_{r,j}$ and $T_{a,j}$ are the tube wall, refrigerant and air temperatures, respectively; $T_{a,j+1}$ and $T_{a,j}$ are the air inlet and outlet temperatures. m_{j-1} (h_{j-1}) and m_j (h_j) represent the inlet and outlet mass flow rates (enthalpy) of refrigerant, respectively. $\dot{m}_{e,j}$ is the time derivative of the refrigerant mass held in the j^{th} control volume; E_j is the tube wall energy and $C_{th,w}$ denotes the thermal capacitance of the heat exchanger's tube wall and fin. Equation 1 characterizes the variation of refrigerant internal energy, while enthalpy allows easier calculation of the heat transfer rate. The time derivative of the refrigerant internal energy in Equation 1 can be decomposed into terms of time derivatives with respect to the pressure and enthalpy:

$$\dot{U}_j = V_j\left(\frac{\partial \rho_j}{\partial P_e}\dot{P}_e + \frac{\partial \rho_j}{\partial h_j}\dot{h}_j\right)h_j - V_j\dot{P}_e + V_j\rho_j\dot{h}_j \tag{4}$$

where V_j and ρ_j represent the tube internal volume and refrigerant density of the j^{th} control volume. The evaporating pressure P_e is assumed to be identical across all control volumes (no pressure drops). Similarly, the mass balance Equation 2 can be re-written as

$$\dot{m}_{e,j} = V_j\dot{\rho}_j = V_j\left(\frac{\partial \rho_j}{\partial P_e}\dot{P}_e + \frac{\partial \rho_j}{\partial h_j}\dot{h}_j\right) \tag{5}$$

Physics-informed empirical correlations are used to calculate the air- and refrigerant-side heat transfer coefficients, i.e., α_a and α_r, while the correlation coefficients were estimated from experimental data. The details of the correlation structure and training process can be found in Liu and Cai (2021b) and are omitted here due to space limitations.

3.1.2 Accumulator

A few assumptions are made for modeling of the accumulator:

- There is no heat gain along the refrigerant line connecting the evaporator and accumulator, i.e., the enthalpy of the accumulator inlet equals that of the evaporator outlet h_N, as this tube section is typically well insulated;
- Outlet enthalpy of the accumulator h_{out} equals the compressor suction enthalpy.
- The heat transfer between the accumulator and its surrounding environment is neglected.

The conservation differential equations for mass and energy of the refrigerant inside the accumulator are

$$\left(\frac{\mathrm{d}\rho_g}{\mathrm{d}P_e}V_g + \frac{\mathrm{d}\rho_f}{\mathrm{d}P_e}V_f\right)\frac{\mathrm{d}P_e}{\mathrm{d}t} + \left(\rho_f - \rho_g\right)\frac{\mathrm{d}V_f}{\mathrm{d}t} = m_{acc} - m_{comp} \tag{6}$$

$$\left(\frac{\mathrm{d}(\rho_g u_g)}{\mathrm{d}P_e}V_g + \frac{\mathrm{d}(\rho_f u_f)}{\mathrm{d}P_e}V_f\right)\frac{\mathrm{d}P_e}{\mathrm{d}t} + \left(\rho_f u_f - \rho_g u_g\right)\frac{\mathrm{d}V_f}{\mathrm{d}t} = m_{acc}h_N - m_{comp}h_{out} \tag{7}$$

where ρ_g (u_g or V_g) and ρ_f (u_f or V_f) are the gas-phase and liquid-phase refrigerant density (specific internal energy or volume in the accumulator), respectively. m_{acc} and m_{comp} are the refrigerant mass flow rates entering the accumulator and the compressor, respectively. The accumulator outlet enthalpy h_{out} is determined by the rules shown in Table 1 (Cheung and Braun, 2014).

Table 1: Outlet refrigerant state for the accumulator

Accumulator inlet state	Liquid level of accumulator	Outlet state
Two phase	Not full	Saturation vapor
	Full	Saturated liquid ("wet compression")
Superheated phase	Empty	Superheated vapor
	Non empty	Saturation vapor

Assuming the total volume of the accumulator is V_{acc}, then $V_{acc} = V_g + V_f$. Using the relationship between the refrigerant specific internal energy and enthalpy ($u = h - \frac{P}{\rho}$), the conservation equations can be reformulated as

$$\begin{bmatrix} \frac{\mathrm{d}\rho_g}{\mathrm{d}P_e}\left(V_{acc} - V_f\right) + \frac{\mathrm{d}\rho_f}{\mathrm{d}P_e}V_f & \rho_f - \rho_g \\ \left(h_g\frac{\mathrm{d}\rho_g}{\mathrm{d}P_e} + \rho_g\frac{\mathrm{d}h_g}{\mathrm{d}P_e}\right)\left(V_{acc} - V_f\right) + \left(h_f\frac{\mathrm{d}\rho_f}{\mathrm{d}P_e} + \rho_f\frac{\mathrm{d}h_f}{\mathrm{d}P_e}\right)V_f - V_{acc} & \rho_f h_f - \rho_g h_g \end{bmatrix}\begin{bmatrix}\dot{P}_e \\ \dot{V}_f\end{bmatrix} = \begin{bmatrix} m_{acc} - m_{comp} \\ m_{acc}h_N - m_{comp}h_{out}\end{bmatrix} \tag{8}$$

where h_g and h_f are the gas-phase and liquid-phase refrigerant enthalpy, respectively.

3.1.3 Integrated low-order (control) model

Let m_{exv} be the refrigerant mass flow through the EXV (or evaporator inlet flow), which relates to the accumulator inlet flow m_{acc} via the following equation

$$m_{acc} = m_{exv} - \left(\dot{m}_{e,1} + \cdots + \dot{m}_{e,N}\right) = m_{exv} - \left[V_1\left(\frac{\partial\rho_1}{\partial P_e}\dot{P}_e + \frac{\partial\rho_1}{\partial h_1}\dot{h}_1\right) + \cdots + V_N\left(\frac{\partial\rho_N}{\partial P_e}\dot{P}_e + \frac{\partial\rho_N}{\partial h_N}\dot{h}_N\right)\right] \tag{9}$$

where N is the number of control volumes in the evaporator.

By combining the governing equations for the evaporator and accumulator, i.e., Equation 3 to Equation 5 and Equation 8, an integrated state-space formulation can be obtained for the evaporator and accumulator set:

$$\mathbf{Z}\underbrace{\begin{bmatrix}\dot{P}_e \\ \dot{h}_1 \\ \vdots \\ \dot{h}_N \\ \dot{T}_{w,1} \\ \vdots \\ \dot{T}_{w,N} \\ \dot{V}_f\end{bmatrix}}_{\dot{\mathbf{x}}} = \underbrace{\begin{bmatrix} m_{exv}\left(h_{in} - h_1\right) + \alpha_{r,1}A_{i,1}\left(T_{w,1} - T_{r,1}\right) \\ \vdots \\ m_{exv}\left(h_{N-1} - h_N\right) + \alpha_{r,N}A_{i,N}\left(T_{w,N} - T_{r,N}\right) \\ m_{exv} - m_{comp} \\ \alpha_{a,1}A_{o,1}\left(T_{eai} - T_{w,1}\right) - \alpha_{r,1}A_{i,1}\left(T_{w,1} - T_{r,1}\right) \\ \vdots \\ \alpha_{a,N}A_{o,N}\left(T_{a,N} - T_{w,N}\right) - \alpha_{r,N}A_{i,N}\left(T_{w,N} - T_{r,N}\right) \\ m_{exv}h_N - m_{comp}h_{out}\end{bmatrix}}_{g(\mathbf{x},\mathbf{u})} \Rightarrow \dot{\mathbf{x}} = \hat{g}\left(\mathbf{x},\mathbf{u}\right) = \mathbf{Z}^{-1}g\left(\mathbf{x},\mathbf{u}\right) \tag{10}$$

where $\mathbf{x}$ is the vector of state variables, $\mathbf{u}$ is the vector of inputs (i.e., $[m_{exv}, m_{comp}, h_{in}, T_{eai}, m_a]$), T_{eai} is the evaporator air inlet temperature, m_a is the evaporator air mass flow rate, h_{in} is the refrigerant enthalpy at evaporator inlet, and $\mathbf{Z}$ is the transformation matrix that is dependent on the evaporation pressure and refrigerant enthalpy of each control volume. The detailed structure of the matrix can be found in Appendix A. This low-order control model for the evaporator and accumulator set is used in the accumulator liquid level estimation and it differs from the high-fidelity plant model (discussed in the next section) in the small number of control volumes for reduced computational demand.

3.2 High-fidelity model for the simulation testbed

To assess the performance and benefits of the proposed estimation and control strategies, a high-fidelity dynamic vapor compression system model has been developed, by extending a previously established gray-box dynamic model for the same test unit described in Liu and Cai (2021a). The high-fidelity model assumes the same structure as described in Section 3.1.1 for the condenser and evaporator but more control volumes are utilized to better capture the system dynamics. Steady-state physics-based models are assumed for characterizing the compressor and EXV behaviors. The model parameters are estimated from experimental data using a hierarchical procedure, in which the steady-state and dynamic model parameters are estimated separately for numerical tractability. Since prior experimental tests always involved a positive superheat with an empty accumulator, the original model described in Liu and Cai (2021a) does not include any accumulator component model. In this study, the accumulator model described in Section 3.1.2 was added to the original system-level dynamic model.

Figure 3 shows the schematics of the high-fidelity and low-order control models. The high-fidelity system model assumes 20 control volumes for both the evaporator and condenser with a simulation time step of 0.01 s. In contrast, the low-order evaporator and accumulator model used for state estimation assumes 5 control volumes with a 0.05 s simulation time step. Note that the low-order control model assumes the same heat transfer correlations (both air- and refrigerant-side) as those involved in the high-fidelity model. In practice, these correlations can be estimated on the fly with field data following the method described in Liu and Cai (2021a). In the simulation tests, the high-fidelity model serves as an emulator of actual systems and the simulated operational variables are used as "measurements" to be fed to the state estimator discussed next.

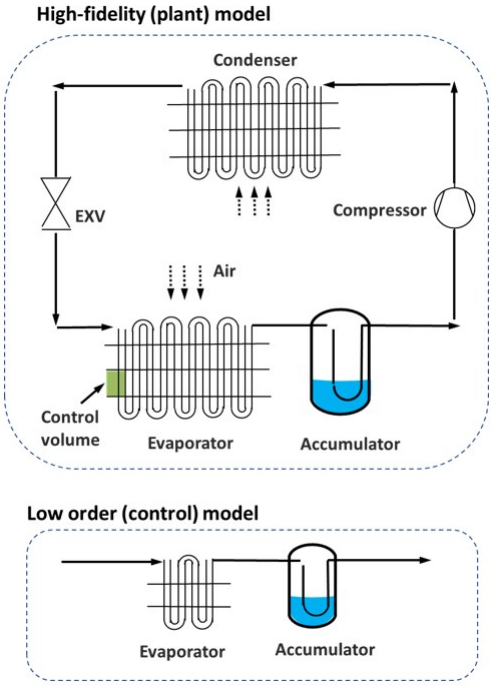

Figure 3: Schematics of the high-fidelity model and the low order model.

4. ACCUMULATOR LIQUID LEVEL ESTIMATOR

The accumulator refrigerant liquid volume V_f, as a state variable of the evaporator-accumulator control model, can be estimated along with other state variables when input/output measurements are available. Since the evaporating pressure P_e is very often monitored in modern air-conditioning and refrigeration systems, it is used as the measurable output variable. When measurements of other operational variables are available, multiple outputs can be used to improve the state estimation accuracy. The input variables, namely $m_{exv}, m_{comp}, h_{in}, T_{eai}$ and m_a, are directly measurable or can be estimated through virtual sensing. Specifically, h_{in} can be measured through pressure and temperature readings at the condenser outlet. The refrigerant mass flow through the EXV and compressor can be estimated with their characteristic curves (e.g., see the methods described in Liu and Cai (2021a)). The evaporator airflow can be inferred from the fan curve while the thermostat temperature can be a proxy for the evaporator inlet air temperature.

We assume that the evaporator-accumulator's dynamics are subjected to the following discrete-time state-space equations with additive noises

$$\mathbf{x}_{k+1} = f(\mathbf{x}_k, \mathbf{u}_k) + \mathbf{w}_k \tag{11}$$

$$y_k = \mathbf{h}^\top \mathbf{x}_k + v_k \tag{12}$$

where $f(\cdot)$ is the discrete-time counterpart of $\hat{g}(\cdot)$, k indicates the time step, $\mathbf{w}_k$ is the process noise subject to a zero-mean normal distribution with a covariance matrix $\mathbf{Q}$, and v_k is the output noise, also assumed to follow a zero-mean Gaussian with a variance R. Since the measured output y is the evaporation pressure P_e, the vector $\mathbf{h}$, which relates the state variables and output, has its first element being unity and all other elements being zero. State estimation can be achieved with the extended Kalman filter, an extension of the classic Kalman filter for nonlinear systems (Hoshiya and Saito, 1984), which estimates the state variables with two sequential steps: next-time-step prediction and update with current output measurement.

Figure 4 depicts the implementation diagram of the state estimator. This study uses naive estimates of the process noise covariance matrix $\mathbf{Q}$ and output variance R based on the respective sensor uncertainties. In practical implementations, more realistic estimates can be obtained through analysis of historical operation data, e.g., using the autocovariance least-squares technique (Rajamani and Rawlings, 2009).

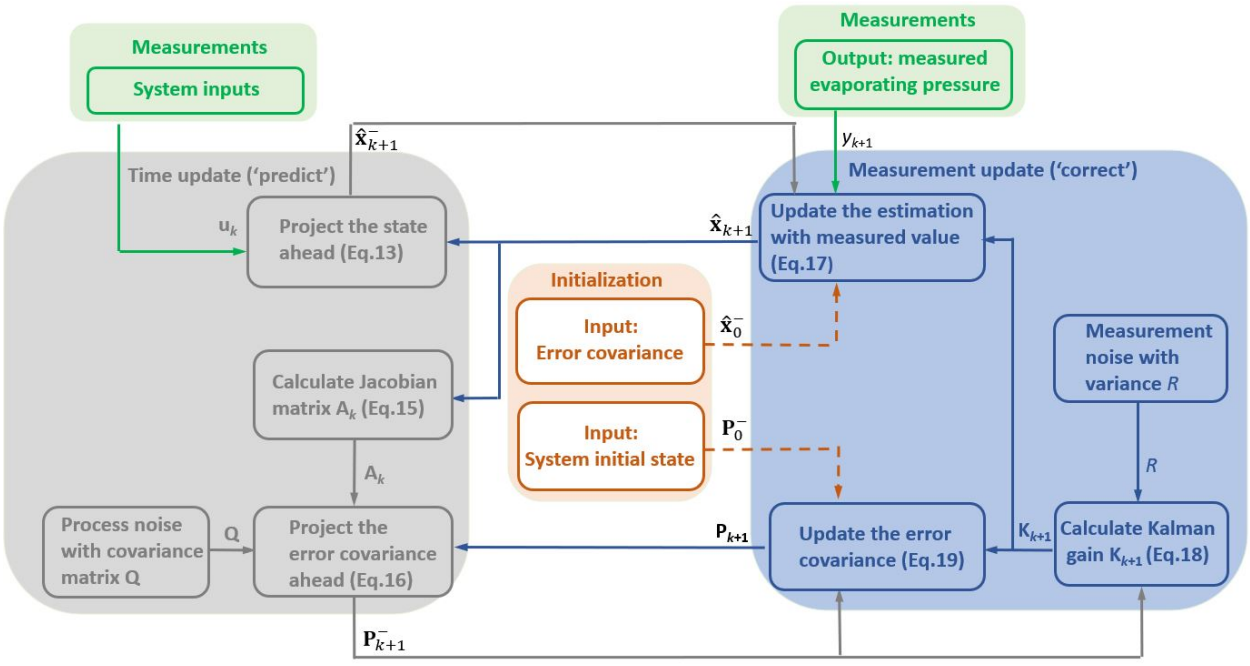

Figure 4: Implementation diagram of the state estimator.

5. ZERO SUPERHEAT AND ACTIVE CHARGE CONTROL

This section describes the zero-superheat and dynamic charge control strategies that can be enabled by the accumulator liquid level estimator.

5.1 Zero-superheat control

It is widely known that lower superheat settings can improve the system COP (Chen et al., 2002, Jensen and Skogestad, 2007, Kim and Braun, 2012, etc), but excessively low superheat may cause control instability and even wet compression that can result in compressor damages. When a suction accumulator is present, a zero superheat setting can be implemented to achieve the maximum efficiency with flooded evaporators, but leads to loss of visibility of the refrigerant status at the evaporator outlet and if the accumulator is completely filled, the compressor will be flooded by pure liquid refrigerant which is disastrous. The proposed accumulator liquid level estimator can fill the visibility gap by affording real-time estimate of the refrigerant liquid level and support a zero-superheat controller to ensure operation safety. In practical implementations, a near-zero superheat setpoint can be used (e.g., 1K in the case study) and the estimated accumulator liquid level can be used to ensure the accumulator is never completely filled. When active charge control is enabled, the zero-superheat condition is automatically satisfied.

5.2 Active charge management

For overcharged systems, the rise of refrigerant mass flow can cause the increase of compressor power consumption and may cause wet compression and jeopardize system reliability. On the other hand, undercharged systems have reduced cooling capacity and degraded system energy efficiency with high superheat. Maintaining an optimum refrigerant charge level is critical to achieve maximum operation efficiency and reliability. Previous studies (Choi and Kim, 2002, Kim and Braun, 2012, Poggi et al., 2008) have revealed concave relationships between the charge level and system COP and the existence of an optimal charge achieving the maximum system COP. However, the charge-COP curve and the optimal charge level vary with operating conditions, especially with the outdoor temperature. The accumulator can serve as a refrigerant reservoir and with proper control, can enable dynamic active charge management, for which real-time estimation of the accumulator liquid level is a prerequisite.

To evaluate the charge-COP relationship of the case study unit, the high-fidelity simulation testbed described in Section 3.2 was run for different ambient temperatures, with the boundary conditions presented in Table 2.

For each simulation test, all the boundary conditions were held constant within a 20-min time window until the system reached steady state. For all the simulation tests, a PI controller was used to modulate the EXV opening to maintain a 1K superheat setpoint. Figure 5 depicts the variation of the steady-state system COP with the ambient temperature and charge level. It can be observed that for a given ambient temperature (T_{cai}), the COP peaks at an intermediate charge level, and the optimal charge level, highlighted in Figure 5, varies and exhibits a positive correlation with the outdoor temperature, which indicates efficiency improvement potentials for dynamic charge management. Specifically, assume the system is charged with 6.4 lbs of refrigerant, which is the optimal charge level for a nominal ambient temperature T_{cai} = 308K; when the ambient temperature drops to 298K, the system becomes overcharged (relative to the optimal charge of 5.35 lbs at the ambient temperature of 298K) and to achieve the maximum operation efficiency during the low temperature hours, the accumulator should store 1.05 lbs (the difference of charge level between T_{cai} = 308K and T_{cai} = 298K) of refrigerant. To achieve dynamic charge control, the EXV can be modulated using a PI controller to maintain the estimated accumulator liquid level on the desired setpoint. Note that the optimal active charge level (equivalently optimal accumulator liquid level) can be determined using a look-up table developed offline or with online optimization techniques such as ESC (Koeln and Alleyne, 2014); finding the optimal active charge is not a focus of this study.

Table 2: Parametric analysis boundary conditions

Operating variables	Indoor temperature (K)	Outdoor temperature (K)	Compressor speed (RPM)	Evaporator air flow rate (CFM)
Setting	298	298, 303, 308, 313	4000	1600

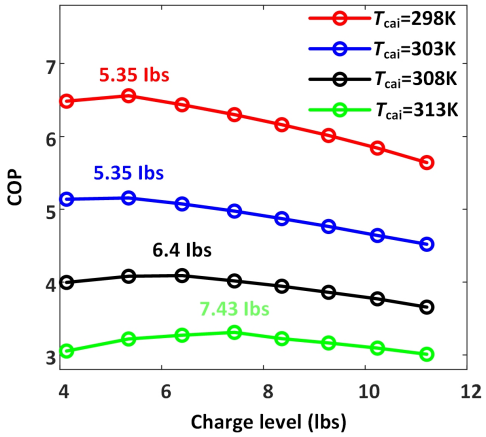

Figure 5: Variation of COP with respect to refrigerant charge level.

6. CONTROL PERFORMANCE VALIDATION

6.1 Simulation-based validation

The accumulator liquid level estimator and the zero-superheat and active charge control strategies were first tested with the high-fidelity simulation testbed described in Section 3.2. It is assumed that the system is charged with 6.4 lbs of refrigerant (optimal charge for T_{cai} = 308K). The boundary conditions were maintained constant in the simulation tests following the settings shown in Table 2 while T_{cai} was fixed to 298K. The simulation test was divided into two stages, with the first stage assessing the COP improvement potential of zero-superheat control and the second stage demonstrating the performance of the active charge management strategy. Figure 6 shows the simulation results.

6.1.1 Zero-superheat control

The P/I gain settings of the original equipment manufacturer (OEM) superheat controller were recovered through offline tests of the EXV, which were determined to be approximately 2 (Step K^{-1}) and 0.01 (Step K^{-1} sec^{-1}), respectively, and used in the simulation test. The test was started with a superheat setpoint of 10K, which was maintained until the system reached steady state. Then the superheat setpoint was reduced to 1K while all boundary conditions and control settings were kept unchanged. A low but non-zero setpoint (1 K) was used to ensure system controllability. The system COP underwent an obvious increase (approximately 8%) with the superheat descent from 10K to 1K, while the accumulator liquid level was zero throughout the first stage (the superheat was positive and no liquid refrigerant entered the accumulator).

6.1.2 Active charge control

Based on the analysis of Section 5.2, the accumulator should hold 1.05 lbs of refrigerant to ensure that the system operates under maximum efficiency. The accumulator in the test unit has a total internal volume V_{acc} of 2.45 L, and the liquid volume of refrigerant in the accumulator can be estimated with

$$\rho_g \left(V_{acc} - V_f\right) + \rho_f V_f = M_{acc} \Rightarrow V_f = \frac{M_{acc} - \rho_g V_{acc}}{\rho_f - \rho_g} \tag{13}$$

where M_{acc} is the desired mass of refrigerant held by the accumulator, i.e., 1.05 lbs. The corresponding accumulator liquid volume is V_f =0.33 L under a nominal evaporation pressure of 1×10^6 Pa.

During the second-stage test, the control strategy switched to the active charge management mode where the regulation variable changed to the estimated refrigerant liquid volume inside the accumulator. Due to the different dynamics between EXV opening and accumulator liquid volume, different PI control gain settings were identified using offline open-loop simulation tests and adopted in the charge control mode. The second-stage test started with a positive superheat of 1K and an empty accumulator at time around 2000 s. When the active charge control mode was enabled, the estimated accumulator liquid volume was zero and below its setpoint of 0.33 L, which drove the EXV to open up allowing more refrigerant flow to the evaporator; this resulted in disappearance of the superheated region and liquid

refrigerant entering the accumulator. The EXV opening was modulated until the accumulator liquid level settled around the setpoint of 0.33 L. The results show a satisfactory agreement between the estimated and actual liquid volume which proves the ability of the state observer approach for accurate estimation of the accumulator liquid volume. With the active charge control, the system COP was boosted by another 2.5%.

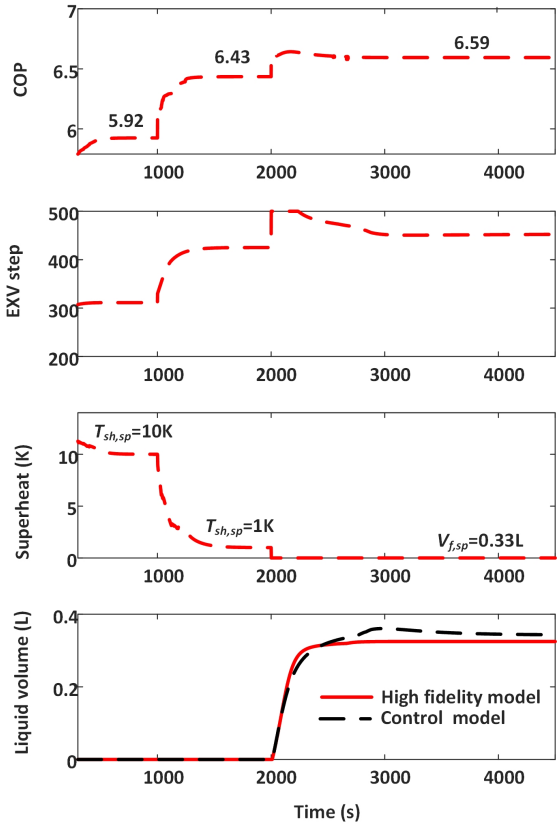

Figure 6: Simulation-based validation results of the estimation and control strategy.

6.2 Experimental validation

Experimental tests were carried out to validate the efficiency improvement potential of the zero-superheat control strategy. All boundary conditions and control settings were kept identical to those involved in the simulation test. Simulations were also carried out with the high-fidelity model to demonstrate the accuracy of the model compared to actual system responses, where the measured boundary conditions were used in the simulations. Note that the charge level of the high-fidelity dynamic model was calibrated in advance with the experimental data by matching the simulated and measured subcooling, a key indicator of refrigerant charge sufficiency.

Figure 7 shows the variations of the system COP, EXV opening, superheat and the simulated accumulator liquid volume. Since there is no liquid level detector in the accumulator, the ground-truth liquid level is unknown. That is why the high-fidelity simulation results are included. The experiment mainly serves to validate the efficiency improvement potential of the zero-superheat controller as no ground-truth charge level is available.

In the tests, a sequence of step changes were imposed on the superheat setpoint, from 10K to 1K with a 3K decrement each step. For each step change, the boundary conditions and control settings were held constant until the system reached steady state. It can be observed the PI controller was able to provide fast responses to the superheat setpoint perturbations and the system COP increased as the superheat was gradually reduced. Reduction of the superheat from 10K to 1K achieved a COP improvement by 6.63% in the experiment. The experimental and simulation results show a good agreement with a simulated COP improvement of 7.5%. In the end of the experiment, the EXV opening was manually increased to 385 steps which drove the superheat to zero and liquid refrigerant to enter the accumulator (liquid

volume V_f increased). This has resulted in a further COP increase of 2.3%, which could be attributed to the superheat reduction from 1K to 0K and active charge management. The exact cause is unknown as the ground-truth charge and accumulator liquid level are not available. However, the experiment has successfully shown the effectiveness and performance of zero-superheat control. Note that during the zero-superheat period, the system pressures and COP underwent minor oscillations, which could be caused by instability of the flow pattern transition in the evaporator (Nayak et al., 2003) and density/thermal oscillations (Liang et al., 2011).

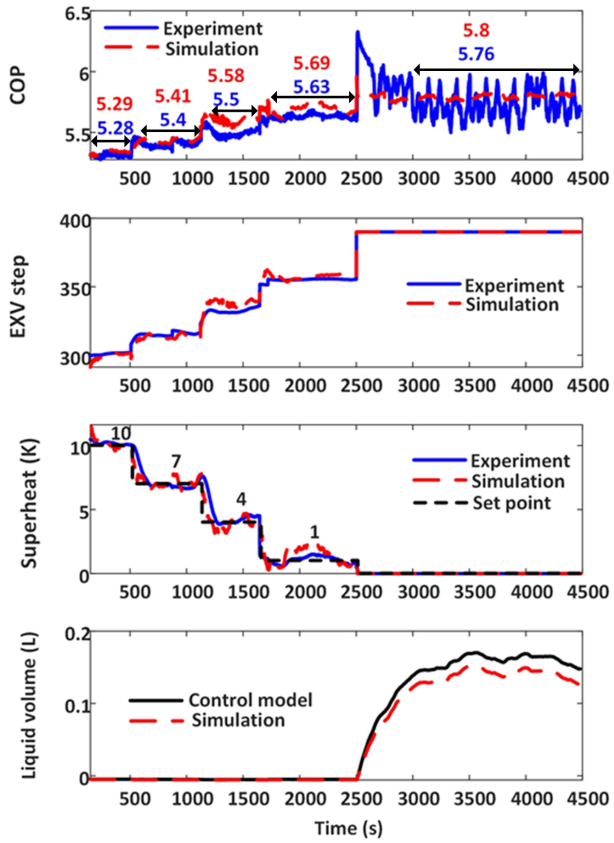

Figure 7: Experimental validation results for the zero-superheat controller.

7. CONCLUSIONS

This paper presented an accumulator liquid level estimation method based on a nonlinear state observer combined with a gray-box dynamic model of the evaporator and accumulator. This method affords a virtual liquid level detection ability from real-time readings of built-in pressure and temperature sensors in modern VCS equipment. The liquid level estimator has particular value in support of zero-superheat and active charge control strategies for energy efficiency improvement. Numerical tests have demonstrated its ability in estimation of the accumulator liquid level for a 3-ton variable-speed heat pump. The numerical results also showed that 8% COP improvement could be achieved by reducing the superheat from 10K to 0K and the COP could be boosted by another 2.5% through active charge management. The experimental tests consolidated the findings from the numerical analysis and a comparable efficiency gain was observed from the zero-superheat and active charge control.

In this study, the extended Kalman filter was used for state estimation which relies on local linearization of the control dynamics around the estimated state point at each time step. Linearization is a computationally demanding step and the non-differentiability of the control model, caused by phase transitions in the evaporator, may cause sub-optimal performance with frequent chattering of the linearized dynamics. An alternative method is to identify a nominal linear surrogate model that recovers most of the control dynamics with minimum instability and computational burden for state estimation. Other state observers with simpler implementations, such as Luenberger observer (Ciccarella et al.,

1993) and sliding mode observer (Davila et al., 2005), can also be explored in future studies. In this analysis, the ground-truth accumulator liquid level was unknown, due to difficulties in installing liquid level detection devices on the test unit. Future work will explore better benchmarking solutions such as addition of sight glass on the accumulator.

REFERENCES

Chen, W., Zhijiu, C., Ruiqi, Z., and Yezheng, W. (2002). Experimental investigation of a minimum stable superheat control system of an evaporator. *International Journal of Refrigeration*, 25(8):1137–1142.

Cheung, H. and Braun, J. E. (2014). Component-based, gray-box modeling of ductless multi-split heat pump systems. *International journal of refrigeration*, 38:30–45.

Choi, J. M. and Kim, Y. C. (2002). The effects of improper refrigerant charge on the performance of a heat pump with an electronic expansion valve and capillary tube. *Energy*, 27(4):391–404.

Ciccarella, G., Dalla Mora, M., and Germani, A. (1993). A luenberger-like observer for nonlinear systems. *International Journal of Control*, 57(3):537–556.

Davila, J., Fridman, L., and Levant, A. (2005). Second-order sliding-mode observer for mechanical systems. *IEEE transactions on automatic control*, 50(11):1785–1789.

EIA (2020). Electricity data. 2020. u.s. https://www.eia.gov/ energyexplained/ electricity/use-of-electricity.php.

Eldredge, B. D., Rasmussen, B. P., and Alleyne, A. G. (2008). Moving-boundary heat exchanger models with variable outlet phase. *Journal of Dynamic Systems, Measurement, and Control*, 130(6):1–12.

Hoshiya, M. and Saito, E. (1984). Structural identification by extended kalman filter. *Journal of engineering mechanics*, 110(12):1757–1770.

Jensen, J. B. and Skogestad, S. (2007). Optimal operation of simple refrigeration cycles: Part i: Degrees of freedom and optimality of sub-cooling. *Computers chemical engineering*, 31(5–6):712–721.

Kim, W. and Braun, J. E. (2012). Evaluation of the impacts of refrigerant charge on air conditioner and heat pump performance. *International journal of refrigeration*, 35(7):1805–1814.

Koeln, J. P. and Alleyne, A. G. (2014). Optimal subcooling in vapor compression systems via extremum seeking control: Theory and experiments. *International journal of refrigeration*, 43:14–25.

Liang, N., Shuangquan, S., Tian, C., and Yan, Y. Y. (2011). Two-phase flow instabilities in horizontal straight tube evaporator. *Applied thermal engineering*, 31(2-3):181–187.

Liu, H. and Cai, J. (2021a). A gray-box dynamic modeling method for variable speed direct-expansion systems. 18th International Refrigeration and Air Conditioning Conference at Purdue.

Liu, H. and Cai, J. (2021b). A robust gray-box modeling methodology for variable-speed direct-expansion systems with limited training data. *International Journal of Refrigeration*, 129:128–138.

Nayak, A. K., Vijayan, P. K., Jain, V., Saha, D., and Sinha, R. K. (2003). Study on the flow-pattern-transition instability in a natural circulation heavy water moderated boiling light water cooled reactor. nuclear engineering and design. *Nuclear engineering and design*, 225(2-3):159–172.

Poggi, F., Macchi-Tejeda, H., Leducq, D., and Bontemps, A. (2008). Refrigerant charge in refrigerating systems and strategies of charge reduction. *International journal of refrigeration*, 31(3):353–370.

Rajamani, M. R. and Rawlings, J. B. (2009). Estimation of the disturbance structure from data using semidefinite programming and optimal weighting. *Automatica*, 45(1):142–148.